

High-resolution measurement of the infrared rotation-vibration spectrum of the negative molecular ion $^{14}\text{NH}^-$

Mohammad Al-Za'al, Harold C. Miller, and John W. Farley

Physics Department and Chemical Physics Institute, University of Oregon, Eugene, Oregon 97403

(Received 8 August 1986)

The authors have performed an extensive series of measurements of the infrared rotation-vibration spectrum of the negative molecular ion $^{14}\text{NH}^-$. A total of 114 transitions in the *P*, *Q*, and *R* branches of the fundamental band near 3000 cm^{-1} have been measured with an accuracy (1 standard deviation) of 0.01 cm^{-1} . The resolution is much higher (7 MHz), enabling us to resolve hyperfine structure. Autodetachment linewidths have also been measured. The electron affinity of NH has been measured with a precision a thousand times higher than previous work: $E_{\text{EA}}(\text{NH}) = 0.374\,362 \pm 0.000\,005\text{ eV}$. Our data agree with earlier measurements of the *R* branch and include the first high-resolution measurements of the *Q* and *P* branches. We have observed rotationally excited metastable states as much as 1.8 eV above the autodetachment threshold. A least-squares fit to the transition frequencies has been performed, using an effective Hamiltonian with a sextic term. The predictions of the best previous work, extrapolated to high *J*, disagree by as much as 10 cm^{-1} , or one thousand times the experimental uncertainty. This paper more than doubles the number of measured transition frequencies in this species.

INTRODUCTION

Molecular ions are very reactive. Consequently, they play an important role in the chemistry of media in which they occur. Negative ions influence the processes of electrical breakdown and current buildup in glow discharges, and are important in laboratory plasmas and in the ionosphere. The continuum absorption in the solar photosphere is strongly affected¹ by the presence of H^- , and some stellar spectra may be affected^{2,3} by the presence of C^- or even² He^- . Negative ions are used in gas chromatography⁴ and tandem accelerators,⁵ and are the basis for the electron-capture detector, used for trace-element analysis. The observed chemical abundances in molecular clouds in the interstellar medium can be reproduced by reactions between positive molecular ions and neutral molecules,⁶ and negative molecular ions may be present in these clouds.^{7,8}

However, the reactive and often fragile character of molecular ions makes their study difficult. The densities of molecular ions obtainable in a discharge are orders of magnitude below the densities of neutral radicals. Only in very recent years have state-resolved spectra of molecular ions been obtained by workers in the field.⁹⁻¹⁶

Negative molecular ions are more difficult to study than positive molecular ions. Early work on negative molecular ions, mostly from the pre-laser-era, has been reviewed by Branscomb,¹⁷ Page and Goode,¹⁸ Berry,¹⁹ and Steiner.²⁰ More recent work has been reviewed by Corderman and Lineberger,⁹ Janousek and Brauman,²¹ Miller,¹⁴ Saykally and Woods,¹³ and Massey.²² Hotop and Lineberger²³ review atomic electron affinities, and Drzagic, Marks, and Brauman²⁴ review molecular electron affinities.

A few negative molecular-ion spectra have been mea-

sured to high resolution. Vibrational structure in O_3^- was observed by Novick *et al.*²⁵ C_2^- has been extensively studied.²⁶⁻²⁹ Schulz *et al.*³⁰ performed a high-resolution (0.2 cm^{-1}) study of the threshold photodetachment of OH^- and OD^- . Dipole-bound states were observed in $\text{H}_2\text{C-CHO}^-$ by Lykke, Mead, and Lineberger³¹ and in FeO^- by Andersen *et al.*³² Bae, Coggiola, and Peterson³³ first observed He_2^- and Michels³⁴ identified the electronic states involved. Saykally and co-workers used a velocity-modulated discharge to discriminate against the much more abundant neutrals, and measured the rotation-vibration spectrum of³⁵ OH^- and³⁶ NH_2^- and also a number of molecular cations. Liu and Oka³⁷ observed the rotational spectrum of OH^- , and Rehfuss, Crofton, and Oka³⁸ observed the rotation-vibration spectrum of OD^- .

The first infrared spectrum of a negative ion was reported recently in the pioneering work of Neumark *et al.*³⁹ They obtained the infrared rotation-vibration spectrum of NH^- in a coaxial ion-beam-laser-beam spectrometer. The transitions are sharp features on the slowly varying background arising from direct photodetachment. They measured 48 *R*-branch transitions with high resolution (better than 20 MHz) and four *Q*-branch transitions with lower resolution. Other high-resolution experiments on positive ions using coaxial beams have been reported by Wing *et al.*⁴⁰ Dufay *et al.*,⁴¹ Carrington and Sarre,⁴² Huber *et al.*⁴³ and Moseley, Olson, and Peterson.⁴⁴

In our experiment we use the coaxial ion-beam-laser-beam technique. We have previously described the first observation⁴⁵ of rotationally excited metastable states of NH^- . Here we review previous work on NH^- and describe the experimental apparatus and procedure. We discuss the equations for Doppler-scanned resonances and the effective Hamiltonian used in analyzing the data. We present our experimental results and our least-squares

analysis of the line centers. We discuss experimental linewidths and intensities, and conclude with some directions for future work.

PREVIOUS WORK ON NH^-

The first experimental study of NH^- was performed by Celotta, Bennett, and Hall,⁴⁶ using a 488-nm Ar^+ laser beam and a crossed-beam apparatus. They produced a very small NH^- beam from an NH_3 discharge and observed one peak in the resulting photoelectron spectrum. Engelking and Lineberger⁴⁷ used a more powerful laser and substituted HN_3 for NH_3 , producing a more intense beam of NH^- . They observed two photoelectron peaks, corresponding to transitions from the $X^2\Pi$ state of NH^- to the $X^3\Sigma^-$ and $a^1\Delta$ states of NH . They obtained an improved value for the electron affinity of NH : 0.381 ± 0.014 eV.

Neumark *et al.*³⁹ used a coaxial-beams apparatus and a color-center laser to study the rotation-vibration spectrum of NH^- . With the laser oscillating on a single cavity mode, they measured transitions in the R branch up to $J=13.5$ with resolution better than 20 MHz. With the laser running multimode, they observed four lines in the Q branch with much lower resolution. The experiment by Newmark *et al.* is discussed in more detail below.

There have been only three theoretical papers on this species. Cade⁴⁸ calculated the electron affinity of NH using a Hartree-Fock technique. Rosmus and Meyer⁴⁹ calculated the electron affinity of NH and the spectroscopic constants and Franck-Condon factors of NH^- , using a sophisticated *ab initio* approach. Recently, Manz *et al.*⁵⁰ used highly correlated wave functions to account for a larger portion of the correlation energy. They obtained spectroscopic constants and infrared transition probabilities for the fundamental and overtone transitions in NH^- and ND^- .

APPARATUS

The apparatus has been described elsewhere in detail,^{51,52} and we give only a brief outline here. A coaxial ion-beam-laser spectrometer is employed, in which rotation-vibration transitions are induced in a beam of NH^- by an infrared beam from a Burleigh FCL-20 color-center laser operating near 3000 cm^{-1} . The vibrationally excited ions then autodetach, and the fast neutral NH is detected. Kinematic velocity compression enables us to achieve a resolution of about 7 MHz [70 parts per 10^9 (ppb)].

NH^- is formed in an active electrical discharge source from the source gas hydrogen azide (HN_3), which is toxic and explosive, and precautions are taken to minimize the hazard. The ion-source inlet gas system uses Clear-Seal⁵³ joints rather than ground-glass joints, and has a Teflon plug for an overpressure safety valve. Only small quantities of hydrogen azide are generated from an aqueous solution (0.5 g/ml) of sodium azide (NaN_3). The reaction vessel is evacuated, then valved off, five drops of concentrated H_2SO_4 are added, and the solution then stabilizes overnight. Adding a few drops of H_2SO_4 in the morning provides a stable supply of HN_3 for the entire day. The

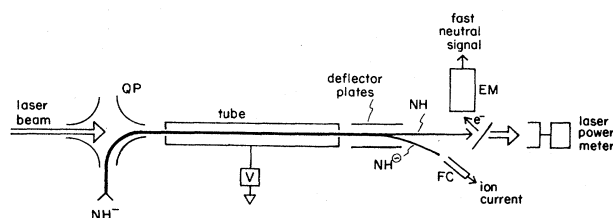


FIG. 1. Schematic diagram of the interaction region. A 2-keV beam of NH^- is deflected by an electrostatic quadrupole (QP) into coincidence with an infrared laser beam. The ions are Doppler tuned by varying the potential on the tube. After ion-laser interaction, the ions are deflected into a Faraday cup (FC). The fast neutrals collide with a plate and produce secondary electrons, which are detected by an electron multiplier (EM).

optimum ion-source conditions are emission current, 1–8 mA; discharge voltage, 100–150 V; and source gas pressure, 20–40 mtorr.

The 2-keV ion beam is extracted from the source, mass-filtered by a Wien filter, and deflected by an electrostatic quadrupole deflector.⁵⁴ Figure 1 shows the interaction region schematically. A tunable infrared beam from a Burleigh FCL-20 color-center laser coaxially overlaps the ion beam in a 50-cm-long equipotential tube, which typically operates near 1 kV above ground, giving a kinetic energy of 3 keV to the ions. Scanning of the spectrometer is accomplished by varying the voltage of the equipotential tube with the laser frequency fixed, thereby Doppler-tuning the ion beam over a 300-V range. Because the differential Doppler shift in our experiment is ~ 10 MHz/V, the 300-V scan corresponds to a frequency scan of ~ 3 GHz (0.1 cm^{-1}).

After interaction with the laser beam, the ions are deflected into a Faraday cup. The NH^- ion current in the cup is typically 1–5 nA. The neutral particles resulting from photodetachment, having essentially the same kinetic energy as the ions, are not deflected significantly. They strike a transparent CaF_2 plate and eject secondary electrons, which are detected by an electron multiplier. The laser beam is mechanically chopped at ~ 600 Hz and the output of the electron multiplier is synchronously detected by a lock-in detector.

PROCEDURE

The laser oscillates on a single cavity mode, selected by an intracavity étalon. In order to avoid intracavity absorption by water-vapor lines, the tuning-arm chamber is evacuated. The frequency range of the experiment ($2941\text{--}3326\text{ cm}^{-1}$) is covered using Burleigh crystal no. 3 (Li:RbCl) pumped with 800 mW of Kr^+ laser (all red) lines. The main tuning element in the laser is the standard B grating which allows laser operation over the range $3015\text{--}3700\text{ cm}^{-1}$. A special A grating is used for tuning over the $2941\text{--}3050\text{ cm}^{-1}$ range. A Burleigh WA-20IR wavemeter is used to measure the laser frequency to an accuracy of 0.01 cm^{-1} . The laser power varies between 2 and 6 mW, depending on the wavelength, of which 35% survives the apertures of the interaction re-

gion. The laser beam is aligned to maximize the laser power through the interaction region, which is measured with a Scientech model 36-2002 power meter.

Using the results of Neumark *et al.*³⁹ as a guide, the expected resonant frequencies in the rest frame of the ion in the *P*, *Q*, and *R* branches were calculated. The corresponding lab frequencies for 3-keV ions were calculated using standard Doppler-shift formulas. During each scan, the laser frequency is kept fixed while the voltage on the equipotential tube, V_e , is varied through 300 V. An S-100-bus microcomputer scans the voltage on the equipotential tube via a digital-to-analog converter, whose (0–10 V) output is amplified and used to program a (0–300 V) Lambda LQD-425 power supply. Fast scans (2.5 V/sec) are used to locate resonances. The laser frequency is adjusted to place the resonance position near 3000 V. The voltage on the equipotential tube has a focusing effect on the ion beam, and affects the geometrical overlap with the laser beam, causing the direct photodetachment signal to vary by $\sim 10\%$ in a 300-V scan. By measuring resonances under standard conditions, we obtain reliable intensity measurements. The precision measurements are made by scanning at 0.3 V/sec for narrow lines and 1 V/sec for broad lines.

Volages proportional to the scan voltage and the lock-in signal are measured by the analog-to-digital converter of the microcomputer. The computer reads the evacuated Burleigh wavemeter via a parallel port, and measures the scan voltage and the lock-in signal, while scanning the ion-beam energy. Data are stored on floppy disks and displayed by a strip-chart recorder. Two lines separated by less than 0.1 cm^{-1} can be observed in a single voltage scan, and their frequency difference measured to an accuracy of $1 \text{ V} (3 \times 10^{-4} \text{ cm}^{-1})$.

THEORY OF DOPPLER-SCANNED RESONANCES

In this section a number of useful formulas are developed, relating quantities measured in the laboratory frame (unprimed) to those measured in the rest frame of the ion (primed). An ion of mass M and charge q is created in the ion source at electrostatic potential V_s , having initial kinetic energy T_s . In the interaction region, the ion has potential energy and kinetic energy given by qV and T . The total energy E is conserved in the electrostatic acceleration process, and therefore

$$T_s + qV_s = T + qV. \quad (1)$$

We neglect the small probability of collision between ions and background gas during extraction. Such collisions will at most produce a small asymmetry to the resonances. V_s is nominally equal to the voltage applied to the anode of the ion source, with small corrections arising from space-charge and similar effects within the ion source; and the width ΔV_s is determined by the variation of the potential over the effective source volume. T_s and ΔT_s are determined by the production mechanism for the ion. V is the voltage on the equipotential tube.

The kinetic energy T is given by special relativity as

$$T = [(1 - \beta^2)^{-1/2} - 1]Mc^2, \quad (2)$$

where $\beta = v/c$. The ion beam overlaps the laser beam at an angle θ , defined so that $\theta = 0$ (π) corresponds to parallel (antiparallel) beams. The laser frequency ν is Doppler shifted to ν' in the ion frame. The two frequencies are related by⁵⁵

$$\nu' = \nu(1 - \beta \cos\theta)(1 - \beta^2)^{-1/2}. \quad (3)$$

In order to obtain ν' as a function of V , we rearrange Eq. (2) to express β as

$$\beta = (2\eta + \eta^2)^{1/2} / (1 + \eta), \quad (4)$$

where the small ratio η is

$$\eta \equiv T/Mc^2. \quad (5)$$

Insertion of Eq. (4) in Eq. (3) then yields

$$\nu' = \nu[1 + \eta - (2\eta + \eta^2)^{1/2} \cos\theta]. \quad (6)$$

From Eqs. (1) and (5), η can be expressed as

$$\eta = [T_s + q(V_s - V)]/Mc^2. \quad (7)$$

Equations (6) and (7) express ν' and the Doppler shift,

$$\Delta\nu = \nu' - \nu, \quad (8)$$

as a function of V . As the voltage of the ion beam is scanned, the ions are Doppler tuned through resonance. The conversion between frequency and voltage, the differential Doppler shift, is given by

$$d\nu'/dV = -(q\nu/Mc^2)[1 - (2\eta + \eta^2)^{-1/2} \times (1 + \eta)\cos\theta]. \quad (9)$$

The equations so far have been relativistically exact. For $\beta \ll 1$, useful approximations are

$$\nu' \cong \nu\{1 - [2(T_s + qV_s - qV)/Mc^2]^{1/2} \cos\theta\}, \quad (10)$$

and

$$d\nu'/dV \cong q\nu[2Mc^2(T_s + qV_s - qV)]^{-1/2} \cos\theta. \quad (11)$$

In our experiment, the numerical values of the relevant quantities are $q(V_s - V) \sim 3 \text{ keV}$, $\cos\theta = 1$, $M = 15 \text{ amu}$, and $\nu \sim 3100 \text{ cm}^{-1}$, yielding $\beta = 6.55 \times 10^{-4}$, $\Delta\nu \sim -2 \text{ cm}^{-1}$, and $d\nu'/dV = -3.4 \times 10^{-4} \text{ cm}^{-1}/\text{V}$ ($\sim -10 \text{ MHz/V}$).

Resolution

The factors which determine the resolution of this experiment are the linewidth of the laser, the divergence of the ion beam, and the velocity spread in the ion beam. The FCL-20 laser has a short-term linewidth which is specified by the manufacturer to be less than 1 MHz ($3.3 \times 10^{-5} \text{ cm}^{-1}$). The narrowest experimental linewidth is $\sim 7 \text{ MHz}$, indicating other broadening mechanisms.

The broadening due to the divergence of the ion beam can be estimated from Eq. (10), subtracting the two extreme values at $\theta = \Delta\phi/2$ and $\theta = 0$, where $\Delta\phi$ is the full-angle divergence of the ion beam. Making the paraxial approximation, $\cos\theta \cong 1 - \theta^2/2$, we have

$$\Delta\nu'_{\text{div}} \cong \nu[2(T_s + qV_s - qV)/Mc^2]^{1/2} (\Delta\phi)^2/8. \quad (12)$$

The 45-cm interaction length and 1.5-mm apertures produce a worst-case divergence of $\Delta\phi = 6.7$ mrad. The resulting contribution to the linewidth is $1.1 \times 10^{-5} \text{ cm}^{-1}$ (330 kHz), which is negligible. By the same argument, the divergence of the laser beam is also unimportant.

Probably the most important factor is the Doppler broadening due to the energy spread in the ion beam, $q\Delta V$, given by Eq. (11) as

$$\Delta v' \cong v[2Mc^2(T_s + qV_s - qV)]^{-1/2}(\cos\theta)q\Delta V, \quad (13)$$

or

$$\Delta v' \cong (10 \text{ MHz}/V)\Delta V. \quad (14)$$

The energy spread of the ions is unchanged as the ions are accelerated but the velocity spread decreases during acceleration,⁵⁶ as shown in Eq. (13).

The observed linewidth is a convolution of the autodetachment linewidth, unresolved hyperfine structure, and the velocity distribution of the ion beam. The first two factors determine the linewidths of all but the narrowest transitions. The full width at half maximum (FWHM) linewidth of the narrowest peak, 7 MHz, sets an upper bound of ~ 0.7 eV on the energy spread, which agrees with experiments by other groups using similar ion sources; studies on C_2^- indicate⁵⁷ that a small energy spread is obtained at low source pressure. Our source pressure is only ~ 30 mtorr, and the small energy spread is not unexpected.

Fine structure of NH^-

The rotational fine structure of NH^- is intermediate between Hund's case-(a) and case-(b) coupling. Hund's coupling cases are discussed in detail by Herzberg.⁵⁸ The angular momenta N , S , and J represent the nuclear rotation, electronic spin, and total angular momentum, respectively. At low J , the coupling is case (a), where L and S are strongly coupled to the internuclear axis, forming the spin-orbit states $^2\Pi_{3/2}$ (F_1 manifold) and $^2\Pi_{1/2}$ (F_2 manifold), respectively. At high J , S decouples from the internuclear axis and the coupling becomes case (b). Figure 2 shows the lowest energy levels of NH^- ($v=0$ and 1). The spin-orbit interval in NH^- is inverted; i.e., the F_1 manifold has lower energy than the F_2 manifold. For high J , F_1 (F_2) levels have $N = J - 0.5$ ($J + 0.5$). Due to Λ doubling, each J level is further split into two sublevels of opposite parity. Sublevels are labeled by e or f following the convention of Brown *et al.*⁵⁹ for molecules with half-integral J ; e levels have parity $(-1)^{J-1/2}$ and f levels have parity $-(-1)^{J-1/2}$. The upper (lower) Λ -doublet levels of F_1 are f (e) levels. In the F_2 manifold, except for $J=0.5$ and 1.5, the upper (lower) Λ -doublet levels are e (f) levels. The parity ordering in the F_2 manifold reverses between $J=1.5$ and 2.5 because of the spin decoupling. The magnitude of the Λ -doublet splitting is larger in the F_1 manifold than in the F_2 manifold.

The electric dipole selection rules are

$$e \rightarrow f \text{ or } f \rightarrow e \text{ for } \Delta J = 0 \quad (15)$$

and

$$e \rightarrow e \text{ or } f \rightarrow f \text{ for } \Delta J = \pm 1. \quad (16)$$

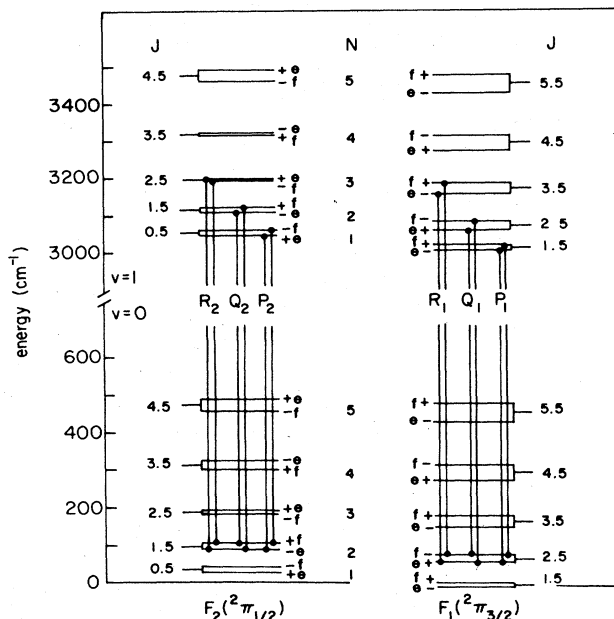


FIG. 2. Energy levels and transitions of NH^- . The variable N is the electronic angular momentum excluding spin. The size of the Λ -doublet intervals is exaggerated for clarity, but otherwise the diagram is drawn to scale.

These follow from the general rule that the parity must change in an electric dipole transition.

MODEL HAMILTONIAN OF NH^-

The molecular orbital configuration of the $^2\Pi_i$ state of NH^- is $(1s\sigma)^2(2s\sigma)^2(2p\sigma)^2(2p\pi)^3$, and that of the excited $^2\Sigma^+$ state is $(1s\sigma)^2(2s\sigma)^2(2p\sigma)(2p\pi)^4$. NH^- is similar to the isoelectronic OH radical, extensively studied by Mailard, Chauville, and Mantz,⁶⁰ Brown *et al.*,⁶¹ Coxon *et al.*,⁶² and Amano.⁶³ A model $^2\Pi$ Hamiltonian with adjustable parameters to fit experimental data has been developed by Zare *et al.*⁶⁴ The parameters for a particular Hamiltonian are effective constants which are only meaningful for that Hamiltonian, and it is important to specify both the Hamiltonian and the fitting constants.

The hyperfine-structure Hamiltonian will not be treated here. The hyperfine splittings are large enough to be resolved by our experimental resolution, but too small to affect the absolute accuracy of the line center of the rotation-vibration transition. This seemingly paradoxical result arises because our experimental accuracy is 0.01 cm^{-1} , set by the limit on our ability to measure the laser frequency, whereas the experimental resolution is much better. Including the hyperfine Hamiltonian and statistically averaging over the hyperfine levels would contribute no significant shift to the rotation-vibration line center.

Neumark *et al.*³⁹ fitted their line-position data to the effective rotational Hamiltonian derived by Zare *et al.*⁶⁴ using a nonlinear least-squares-fitting program. In order to facilitate comparison we will use the same model Hamiltonian, with an additional sextic term needed for our more extensive data.

The case-(a) matrix elements are given by⁶⁴

$$\begin{aligned} \langle {}^2\Pi_{3/2} | H | \Pi_{3/2} \rangle = & T_v + B_v(x^2 - 2) + \frac{1}{2}A_v - D_v[(x^2 - 2)^2 + (x^2 - 2) + 1] \\ & + H_v[(x^2 - 2)^3 + (x^2 - 1)(3x^2 - 4)] + \frac{1}{2}a_D + \frac{1}{2}A_D(x^2 - 2) + \frac{1}{2}q_v(x^2 - 1), \end{aligned} \quad (17)$$

$$\begin{aligned} \langle {}^2\Pi_{1/2} | H | {}^2\Pi_{1/2} \rangle = & T_v + B_v x^2 - \frac{1}{2}A_v - \gamma_v - D_v(x^4 + x^2 - 1) + H_v[x^6 + (x^2 - 1)(3x^2 - 2)] \\ & + a_D/2 - A_D x^2/2 + p_v(1 \mp x)/2 + q_v(1 \mp x)^2/2, \end{aligned} \quad (18)$$

and

$$\langle {}^2\Pi_{3/2} | H | {}^2\Pi_{1/2} \rangle = \{ (B_v - \gamma_v/2) - 2D_v(x^2 - 1) + H_v[x^4 + (x^2 - 1)(2x^2 - 3)] + [p_v/4 + q_v(1 \mp x)/2] \} (x^2 - 1)^{1/2}, \quad (19)$$

where $x = J + \frac{1}{2}$, and the upper (lower) sign refers to e (f) parity. This choice of sign is correct when the ${}^2\Pi$ state interacts with a ${}^2\Sigma^+$ state, which is the case for NH^- . If the ${}^2\Sigma$ state were ${}^2\Sigma^-$ rather than ${}^2\Sigma^+$, the signs would be reversed. We simplify Eqs. (17)–(19) by omitting the small term γ_D and by including a_D in T_v .

There are two processes leading to detachment: excitation of the ion, followed by autodetachment, or direct photodetachment. The amplitudes for these two processes can interfere, giving rise to an asymmetric line shape. Our observed resonances show very little asymmetry. In addition, the resonant signal is much stronger than the direct detachment signal. This indicates that the interference is not important. The weak asymmetries observed in some resonances probably arise from an asymmetric velocity profile of the ion beam.

The best discussion of autodetachment dynamics in this species is by Neumark *et al.*³⁹ They tentatively concluded that the upper Λ doublets decay by rotationally promoted vibrational autodetachment, while the situation is less clear for the lower Λ doublets.

RESULTS

A total of 114 rotation-vibration transitions have been measured in the range 2941–3326 cm^{-1} . The signal-to-noise ratio for the strongest lines is about 900 with a lock-in time constant of 400 msec, consistent with a maximum count rate of 10^6 sec^{-1} and a noise level that is nearly shot-noise limited. The signals are strong enough to be visible on an oscilloscope without a lock-in amplifier.

The spectrum consists of rotation-vibration transitions from $v=0 \rightarrow 1$, followed by autodetachment from the $v=1$ level. A total of 80 R -branch transitions were measured, with the two Λ -doublets being well resolved except for the blended R_2 ($J=0.5$) $e \rightarrow e$ and $f \rightarrow f$ transitions. The higher-energy Λ -doublet transitions, terminating on the upper Λ doublet of the $v=1$ manifold, have linewidths that increase rapidly with J . This makes the resonances more difficult to observe experimentally using the voltage-scanning technique, because the resonance widths can exceed the $\sim 0.1 \text{ cm}^{-1}$ scanning range. We measured the broad R -branch transitions only up to $J=5.5$.

The linewidths of the transitions terminating on the lower Λ -doublet levels are narrow, independent of rotational energy. For N'' greater than 13, the $v=0$ states of

the ions in the beam have rotational energies above the autodetachment threshold. We detected these rotationally excited metastable levels up to $N''=35$, which is 1.8 eV into the autodetachment continuum.

The observed (1-0) band structure is shown in Fig. 3. The lines are labeled by N'' . A total of 31 Q -branch transitions were measured with J up to 10.5. We also measured three lines in the P branch, two of which overlap: (P_2 , $J=1.5$, $e \rightarrow e$ and $f \rightarrow f$). Intercombination transitions (transitions from one fine-structure manifold to another) are apparently very weak; we looked for them unsuccessfully. Figure 3 shows only 53 lines out of the 114 lines measured in the experiment because most fine-structure splittings and all Λ -doublet splittings are unresolved on the resolution of the figure. The R_1 and R_2 branches exhibit bandheads at $N''=17$, separated by 0.132 cm^{-1} .

The Q_2 branch transitions begin at a slightly higher energy than the Q_1 branch. The frequencies of the transitions decrease with N . The Λ -doublet splitting in the Q_1 transitions increases more rapidly with N than in the Q_2 transitions. The transitions Q_2 (2.5 , $e \rightarrow f$ and $f \rightarrow e$) overlap. The observed and fitted line positions (discussed below) are given in Table I and labeled by J'' value.

Comparison with other work

Neumark *et al.*³⁹ observed R -branch transitions for J up to 13.5. They observed at low resolution the first four

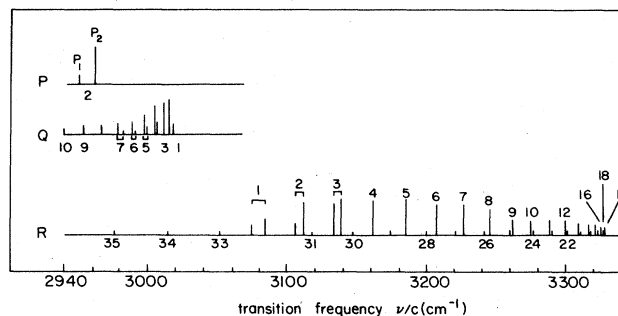


FIG. 3. Stick spectrum of the transitions reported in this work, labeled by the value of N'' . For low N'' , the fine structure transitions are shown separately on the diagram. For higher N'' , the transitions are resolved in the experiment but overlap on the diagram. Not shown in the diagram are Λ -doublet splittings, also experimentally resolved.

TABLE I. Transition frequencies observed in the 1-0 band of $^{14}\text{NH}^-$. Also listed are the results of a least-squares fit to the experimental data.

Transition	Expt. (cm^{-1})	Frequency in ionic rest frame	
		Fit (cm^{-1})	(expt. - fit) $\times 1000$
R_1 (1.5, $f \rightarrow f$)	3085.715	3085.712	3
R_1 (1.5, $e \rightarrow e$)	3085.627	3085.626	1
R_1 (2.5, $f \rightarrow f$)	3112.208	3112.204	4
R_1 (2.5, $e \rightarrow e$)	3112.096	3112.087	9
R_1 (3.5, $f \rightarrow f$)	3137.902	3137.899	3
R_1 (3.5, $e \rightarrow e$)	3137.771	3137.763	8
R_1 (4.5, $f \rightarrow f$)	3162.384	3162.381	3
R_1 (4.5, $e \rightarrow e$)	3162.240	3162.235	5
R_1 (5.5, $f \rightarrow f$)	3185.435	3185.435	0
R_1 (5.5, $e \rightarrow e$)	3185.282	3185.286	-4
R_1 (6.5, $e \rightarrow e$)	3206.796	3206.794	2
R_1 (7.5, $e \rightarrow e$)	3226.665	3226.676	-11
R_1 (8.5, $e \rightarrow e$)	3244.852	3244.873	-21
R_1 (9.5, $e \rightarrow e$)	3261.333	3261.334	-1
R_1 (10.5, $e \rightarrow e$)	3275.999	3276.016	-17
R_1 (11.5, $e \rightarrow e$)	3288.866	3288.881	-15
R_1 (12.5, $e \rightarrow e$)	3299.880	3299.892	-12
R_1 (13.5, $e \rightarrow e$)	3309.002	3309.014	-12
R_1 (14.5, $e \rightarrow e$)	3316.216	3316.216	0
R_1 (15.5, $e \rightarrow e$)	3321.477	3321.467	10
R_1 (16.5, $e \rightarrow e$)	3324.734	3324.737	-3
R_1 (17.5, $e \rightarrow e$)	3326.002	3325.997	5
R_1 (18.5, $e \rightarrow e$)	3325.228	3325.220	8
R_1 (19.5, $e \rightarrow e$)	3322.381	3322.379	2
R_1 (20.5, $e \rightarrow e$)	3317.452	3317.448	4
R_1 (21.5, $e \rightarrow e$)	3310.398	3310.403	-5
R_1 (22.5, $e \rightarrow e$)	3301.210	3301.217	-7
R_1 (23.5, $e \rightarrow e$)	3289.860	3289.866	-6
R_1 (24.5, $e \rightarrow e$)	3276.322	3276.327	-5
R_1 (25.5, $e \rightarrow e$)	3260.565	3260.575	-10
R_1 (26.5, $e \rightarrow e$)	3242.575	3242.585	-10
R_1 (27.5, $e \rightarrow e$)	3222.323	3222.334	-11
R_1 (28.5, $e \rightarrow e$)	3199.792	3199.796	-4
R_1 (29.5, $e \rightarrow e$)	3174.944	3174.945	-1
R_1 (30.5, $e \rightarrow e$)	3147.763	3147.755	8
R_1 (31.5, $e \rightarrow e$)	3118.206	3118.199	7
R_1 (32.5, $e \rightarrow e$)	3086.263	3086.248	15
R_1 (33.5, $e \rightarrow e$)	3051.893	3051.871	22
R_1 (34.5, $e \rightarrow e$)	3015.049	3015.037	12
R_1 (35.5, $e \rightarrow e$)	2975.706	2975.712	-6
R_2 (0.5, $e \rightarrow e$)	3074.618	3074.617	1
R_2 (0.5, $f \rightarrow f$)	3074.618	3074.620	-2
R_2 (1.5, $e \rightarrow e$)	3105.813	3105.821	-8
R_2 (1.5, $f \rightarrow f$)	3105.773	3105.778	-5
R_2 (2.5, $e \rightarrow e$)	3133.985	3133.981	4
R_2 (2.5, $f \rightarrow f$)	3133.912	3133.907	5
R_2 (3.5, $e \rightarrow e$)	3159.824	3159.817	7
R_2 (3.5, $f \rightarrow f$)	3159.726	3159.722	4
R_2 (4.5, $e \rightarrow e$)	3183.671	3183.669	2
R_2 (4.5, $f \rightarrow f$)	3183.562	3183.560	2
R_2 (5.5, $e \rightarrow e$)	3205.671	3205.672	-1
R_2 (5.5, $f \rightarrow f$)	3205.554	3205.558	-4
R_2 (6.5, $f \rightarrow f$)	3225.755	3225.762	-7
R_2 (7.5, $f \rightarrow f$)	3244.168	3244.178	-10
R_2 (8.5, $f \rightarrow f$)	3260.788	3260.793	-5
R_2 (9.5, $f \rightarrow f$)	3275.594	3275.586	8
R_2 (10.5, $f \rightarrow f$)	3288.532	3288.533	-1
R_2 (11.5, $f \rightarrow f$)	3299.607	3299.605	2

TABLE I. (Continued).

Transition	Frequency in ionic rest frame		
	Expt. (cm ⁻¹)	Fit (cm ⁻¹)	(expt. - fit) × 1000
R ₂ (12.5, f → f)	3308.784	3308.774	10
R ₂ (13.5, f → f)	3316.023	3316.011	12
R ₂ (14.5, f → f)	3321.297	3321.289	8
R ₂ (15.5, f → f)	3324.595	3324.579	16
R ₂ (16.5, f → f)	3325.870	3325.855	15
R ₂ (17.5, f → f)	3325.105	3325.090	15
R ₂ (18.5, f → f)	3322.271	3322.258	13
R ₂ (19.5, f → f)	3317.340	3317.334	6
R ₂ (20.5, f → f)	3310.300	3310.292	8
R ₂ (21.5, f → f)	3301.107	3301.109	-2
R ₂ (22.5, f → f)	3289.761	3289.760	1
R ₂ (23.5, f → f)	3276.219	3276.221	-2
R ₂ (24.5, f → f)	3260.459	3260.468	-9
R ₂ (25.5, f → f)	3242.461	3242.477	-16
R ₂ (26.5, f → f)	3222.210	3222.224	-14
R ₂ (27.5, f → f)	3199.675	3199.683	-8
R ₂ (28.5, f → f)	3174.831	3174.829	2
R ₂ (29.5, f → f)	3147.640	3147.636	4
R ₂ (30.5, f → f)	3118.078	3118.076	2
R ₂ (31.5, f → f)	3086.133	3086.121	12
R ₂ (32.5, f → f)	3051.747	3051.740	7
R ₂ (33.5, f → f)	3014.893	3014.902	-9
R ₂ (34.5, f → f)	2975.547	2975.572	-25
Q ₁ (1.5, e → f)	3019.439	3019.420	19
Q ₁ (1.5, f → e)	a	3019.325	
Q ₁ (2.5, e → f)	3016.719	3016.720	-1
Q ₁ (2.5, f → e)	3016.426	3016.422	4
Q ₁ (3.5, e → f)	3012.683	3012.683	0
Q ₁ (3.5, f → e)	3012.077	3012.084	-7
Q ₁ (4.5, e → f)	3007.298	3007.281	17
Q ₁ (4.5, f → e)	3006.281	3006.293	-12
Q ₁ (5.5, e → f)	3000.508	3000.510	-2
Q ₁ (5.5, f → e)	2999.039	2999.048	-9
Q ₁ (6.5, e → f)	2992.367	2992.370	-3
Q ₁ (6.5, f → e)	2990.337	2990.354	-17
Q ₁ (7.5, e → f)	2982.860	2982.865	-5
Q ₁ (7.5, f → e)	2980.194	2980.213	-19
Q ₁ (8.5, f → e)	2968.617	2968.630	-13
Q ₁ (9.5, f → e)	2955.607	2955.606	1
Q ₁ (10.5, f → e)	2941.179	2941.146	33
Q ₂ (0.5, e → f)	3019.969	3019.963	6
Q ₂ (0.5, f → e)	3019.871	3019.865	6
Q ₂ (1.5, e → f)	3017.248	3017.244	4
Q ₂ (1.5, f → e)	3017.148	3017.143	5
Q ₂ (2.5, e → f)	3012.956	3012.948	8
Q ₂ (2.5, f → e)	3012.956	3012.953	3
Q ₂ (3.5, e → f)	3007.170	3007.174	-4
Q ₂ (3.5, f → e)	3007.381	3007.383	-2
Q ₂ (4.5, e → f)	2999.950	2999.952	-2
Q ₂ (4.5, f → e)	3000.451	3000.453	-2
Q ₂ (5.5, e → f)	2991.280	2991.291	-11
Q ₂ (5.5, f → e)	2992.159	2992.167	-8
Q ₂ (6.5, e → f)	2981.180	2981.192	-12
Q ₂ (7.5, e → f)	2969.651	2969.658	-7
Q ₂ (8.5, e → f)	2956.701	2956.691	10
P ₁ (2.5, f → f)	2950.233	2950.216	17
P ₁ (2.5, e → e)	a	2950.333	
P ₂ (1.5, e → e)	2962.495	2962.489	6
P ₂ (1.5, f → f)	2962.495	2962.489	6

^aNot observed.

TABLE II. Our experimental measurements and the results of our least-squares fit, compared with those of Neumark *et al.* for the $N''=13$ transitions in the R branch. The discrepancy is discussed in the text.

Transition	Experiment	Fit	(expt. - fit) $\times 1000$	Ref.
R_1 (13.5, $e \rightarrow e$)	3309.21(1)	3308.996	214	39
	3309.002(10)	3309.014	-12	this work
R_2 (12.5, $f \rightarrow f$)	3308.996(2)	3308.767	229	39
	3308.784(10)	3308.774	10	this work

lines in the Q branch and none in the P branch. Our results agree with theirs with an rms deviation of 0.013 cm^{-1} , which is within the experimental uncertainty.

There are, however, two R -branch transitions ($N''=13$) for which our data disagree significantly with those of Neumark (Table III of Neumark, our Table II). The measurements by Neumark *et al.*³⁹ disagree with our measurements, and with their least-squares fit. Neumark *et al.* excluded these two data from their fit, because their inclusion degraded the fit. We also excluded them in the comparison of the two data sets. Probably the transition found by Neumark at 3308.996 cm^{-1} and identified as R_2 (12.5, $f \rightarrow f$) was misidentified, and is actually R_1 (13.5, $e \rightarrow e$). This brings their observed transition into agreement with our experimental measurement and with the least-squares fit of both groups. One must then attribute the resonance Neumark found at 3309.21 cm^{-1} to a spurious effect (e.g., a laser-mode hop). With the benefit of hindsight, and the new experimental measurements, it is clear that nothing unusual happens at $N''=13$.

We note in passing two minor discrepancies with the Neumark paper. Their off-diagonal matrix element differs in sign from our own, Eq. (19). Because this matrix element is squared in the analysis of the fine-structure energy levels, it makes no difference to the fine-structure energy, but it affects the wave function, and will matter when evaluating hyperfine energies. Our expression is consistent with that of Zare *et al.*⁶⁴ Secondly, there is a typographical error in Table III of Neumark *et al.* for the R_1 (6.5, $e \rightarrow e$) transition, which should read 3206.768 cm^{-1} .

ANALYSIS

Least-squares fit to transition frequency data

A least-squares fit was performed to the experimental line centers, using the model Hamiltonian described above. The least-squares fit was performed on a PDP-10 computer and implemented using a FORTRAN program based on the CURFIT subroutine,⁶⁵ suitable for functions that are nonlinear in their parameters, based on the search algorithm of Marquardt.⁶⁶ The program adjusts the parameters to minimize the reduced χ^2 , which is the mean-square deviation of the fit, measured in terms of the putative experimental uncertainties and averaged over the data set. We assigned equal experimental uncertainties of 0.01 cm^{-1} for all data points.

Correctly estimated experimental uncertainties and a perfect model Hamiltonian would produce a reduced χ^2 of unity. The reduced χ^2 returned by the fitting program was 1.04 (101 degrees of freedom), indicating that the data are under good statistical control. The optimized parameters returned by the fit are compared with the parameters obtained by Neumark *et al.*³⁹ in Table III. The value of A_D returned by a preliminary run of the fitting program was not significantly different from zero, and it was omitted in the final fit (Table III).

The least-squares fit performed by Neumark *et al.*³⁹ included lines in the R branch up to $J=12.5$, whereas the fit in this work includes additional lines in the R branch up to $J=35.5$, 31 lines in the Q branch, and the first two lines in the P branch. The more extensive data set, in-

TABLE III. Optimized parameters for $^{14}\text{NH}^-$. Our constants are quoted to enough significant figures to reproduce all transition frequencies to within the experimental uncertainty of 0.01 cm^{-1} .

Parameter (cm^{-1})	$v=0$		$v=1$	
	This work	Ref. 39	This work	Ref. 39
T	0	0	3020.3974(22)	3020.36(1)
B	16.226 622(418) ^a	16.240(4) ^a	15.520 438(359)	15.529(3)
A	-48.4264(370)	-48.83(11)	-48.8737(386)	-49.34(14)
$10^3 D$	1.779 606(4000)	1.70(5)	1.762 928(3000)	1.68(4)
$10^7 H$	1.751 15(6461)		1.595 06(6000)	
A_D	0		0	
$10^2 p$	9.219(66)	8.9(4)	8.413(63)	8.1(4)
$10^2 q$	-2.1214(109)	-2.13(5)	-1.8167(88)	-1.82(4)

^aValues in parentheses represent one standard deviation in the fit.

cluding the important Q branch, reduces the correlated errors of the fitting parameters. The uncertainties in the fitting parameters are lower than those of Neumark *et al.* by factors ranging from 3 to 17. Our high- J data allowed us to determine the sextic parameter H_v for the first time, which becomes important for large values of J . The fit of Neumark *et al.*, based entirely on a data set with $J \leq 12.5$, extrapolates poorly to quantum states with high values of J ; the deviation between our new measurements and the extrapolated calculated values is as large as 10 cm^{-1} , or a thousand experimental standard deviations.

There are minor differences between the values of the parameters obtained in this work and by Neumark *et al.*³⁹ These differences are not surprising, and arise for well-known reasons: the optimized parameters depend on the range of the quantum numbers in the data set and on the number of terms in the Hamiltonian. This stems from the following two facts: (1) the terms in the Hamiltonian are not orthogonal, and therefore different terms act as proxies for each other; and (2) different terms have different sensitivities to data with low or high J . The fitting parameters are merely a convenient way of reproducing the energy levels; it is the energy levels that are real, not the parameters. The most meaningful comparison is not between our fitting parameters and those of Neumark *et al.*³⁹ but between our transition frequencies and theirs, discussed above.

Evaluation of equilibrium spectroscopic constants

Equilibrium spectroscopic constants can be obtained from the optimized fitted constants B_v , D_v , and H_v , defined by

$$B_v = B_e - \alpha_e(v + \frac{1}{2}), \quad (20)$$

$$D_v = D_e + \beta_e(v + \frac{1}{2}), \quad (21)$$

and

$$H_v = H_e + \eta_e(v + \frac{1}{2}). \quad (22)$$

The internuclear separation r_e is given by

$$B_e = h / (8\pi^2 c \mu r_e^2), \quad (23)$$

where μ is the reduced mass. The spectroscopic constants obtained from Eqs. (20)–(23) are listed in Table IV, with uncertainties calculated using the correlation matrix.⁶⁵ The table also shows the results of Neumark *et al.*³⁹ and the calculations of Rosmus and Meyer⁴⁹ and of Manz

*et al.*⁵⁰ Our values are in agreement with the values of Neumark *et al.*³⁹ Our equilibrium constants have improved accuracy because they are extracted from improved fitting constants. Higher-order correction coefficients, being small differences of fitting constants, are especially sensitive to uncertainties in the fitting constants. Four such constants listed in Table IV are obtained for the first time. The agreement with the theoretical values^{49,50} is not quite as good.

The value of D_e , the centrifugal distortion parameter, can be compared with the expression⁵⁸ based on a harmonic oscillator model,

$$D_e = 4B_e^3 / \omega_e^2. \quad (24)$$

We use the experimental value for T_1 from Table III and the theoretical value⁵⁰ for $\omega_e x_e$ to estimate $\omega_e = 3198.4 \text{ cm}^{-1}$, which yields $D_e \sim 1.782 \times 10^{-3} \text{ cm}^{-1}$, in agreement with the experimental result in Table IV within 0.3%. This shows that the harmonic-oscillator model is quite good for the potential well, even though significant deviation might be expected in a data set including high- J states.

Search for systematic errors in the line centers

We repeated the measurements for 10 narrow lines with the laser beam antiparallel to the ion beam. The frequencies with antiparallel beams were consistently lower than the data with parallel beams; the differences ranged from 0.007 to 0.033 cm^{-1} with an rms average of 0.023 cm^{-1} . Such a systematic error could arise from a hypothetical -30-V offset in the beam voltage. There was no evidence for a systematic error larger than 0.01 cm^{-1} , which is the readout limit of the Burleigh wavemeter. In view of the small size and uncertain interpretation of this possible systematic error, further investigation of it is not warranted. A nice calibration point is provided by the ions themselves because our measurements agree with those of Neumark *et al.*³⁹ who used antiparallel beams, within 0.013 cm^{-1} .

Linewidth analysis

The resonance linewidths are displayed as a function of N'' in Fig. 4. The lower figure shows the linewidths of transitions to F_1 (e) levels and F_2 (f) levels. The $v=1$ levels are the lower Λ -doublet levels, except for $N''=1$ and 2 in the F_2 manifold. The linewidths of the transitions R_1 ($e \rightarrow e$) and R_2 ($f \rightarrow f$) are independent of N'' .

TABLE IV. Spectroscopic constants of $^{14}\text{NH}^-$. All constants except r_e are in cm^{-1} .

Quantity	This work	(Ref. 39)	(Ref. 49)	(Ref. 50) ^a
α_e	0.706 18(14)	0.712	0.691	0.731
B_e	16.579 71(46)	16.607	16.61	16.48
r_e (Å)	1.039 94(2)	1.039	1.039	1.043
β_e	$-1.67(11) \times 10^{-5}$			
D_e	$1.7879(41) \times 10^{-3}$			
H_e	$1.83(7) \times 10^{-7}$			
η_e	$-1.56(4) \times 10^{-8}$			

^aThese values are regarded by the authors of Ref. 50 as their most reliable.

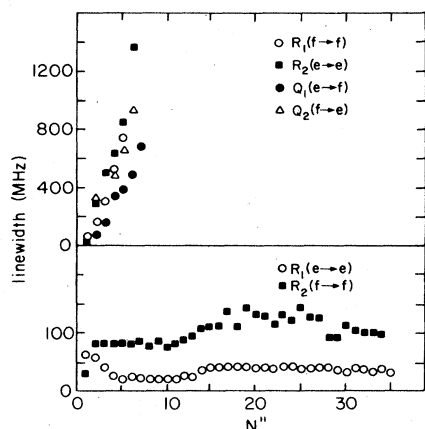


FIG. 4. Experimental linewidths of resonances. Upper (lower) graph shows transitions to upper (lower) Λ -doublet levels.

The upper figure shows transitions to the upper Λ -doublet levels, which increases by a factor of 4 as N'' varies from 2 to 5. The corresponding lifetimes decrease from 0.8 to 0.2 ns.

The linewidth data provide only a lower bound for the autodetachment lifetimes, because the observed linewidths have contributions from unresolved hyperfine structure (hfs) and the velocity spread in the ion beam. The linewidths of the R_1 ($e \rightarrow e$) transitions (except at low N'' where hfs satellite lines broaden the spectrum) are 20–40 MHz. The lower bounds on lifetimes are 7.95–3.98 ns. The R_2 ($f \rightarrow f$) transitions (except at very low N'') have 70–120-MHz linewidths, yielding 2.27–1.33-ns lifetimes. The linewidth data in the Q branch are limited to $N'' \leq 10$. As in the R branch, the Q -branch transitions to the lower Λ -doublet levels maintain approximately the same width for all values of N'' . In the Q branch the hyperfine structure is large because of the pronounced difference between the hyperfine splittings in the initial e (f) and final f (e) states. The Q_2 ($e \rightarrow f$) linewidths are in the range 220–270 MHz, while the Q_1 ($f \rightarrow e$) linewidths are in the 70–120-MHz range. The corresponding lifetimes are 0.72–0.59 nsec and 2.27–1.36 nsec, respectively. The Q_1 ($e \rightarrow f$) and Q_2 ($f \rightarrow e$) transitions to upper Λ -doublet states broaden rapidly with increasing N'' as in the R branch. A common feature between the linewidth data in the R and Q branches is that the linewidths of transitions are larger for the F_2 manifold than for the F_1 manifold. Good agreement is found with the linewidth measurements of Neumark *et al.*³⁹

Discussion of experimental line shapes

Figures 5 and 6 show Q_2 (0.5) $e \rightarrow f$ and $f \rightarrow e$, respectively. The line shapes are similar except for the higher resolution in the former case; each consists of two peaks or groups of peaks separated by ~ 190 MHz. The e and f levels differ substantially in lifetimes even at the lowest possible J . The short-lived e level lies energetically below the f level for $J = \frac{1}{2}$ of the $v = 1$ F_2 manifold, whereas at high values of J the long-lived states are the lower Λ dou-

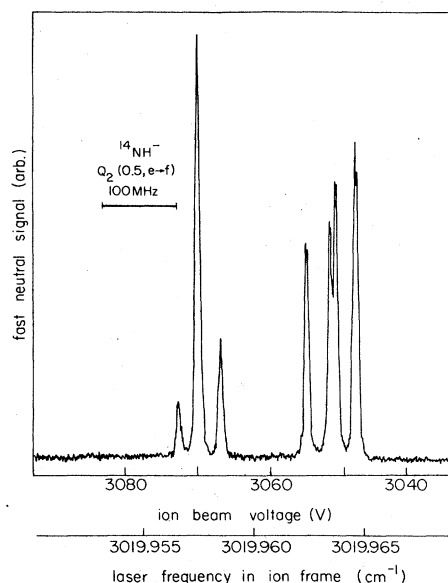


FIG. 5. Experimental line shape of the Q_2 (0.5) $e \rightarrow f$ transition.

blets of the F_1 and F_2 manifolds.

Figure 7 shows two blended R -branch transitions, the R_2 (0.5) $e \rightarrow e$ and $f \rightarrow f$. The line shape consists of a broad (~ 200 MHz) peak at lower frequency and four narrower (~ 30 MHz) peaks at higher frequency. The narrower peaks belong to the $f \rightarrow f$ transitions, because the width of the individual peaks matches the Q_2 (1.5, $e \rightarrow f$) widths, which terminate on the same upper level.

Figure 8 shows the blended P_2 (1.5, $e \rightarrow e, f \rightarrow f$) transitions. The Q_2 (0.5, $e \rightarrow f$ and $f \rightarrow e$) transitions (Figs. 5 and 6) involve the same upper states as those in Fig. 8. Based on the much narrower width of the upper f levels, Fig. 8 must consist of a broader $e \rightarrow e$ peak at lower frequency and a group of narrower $f \rightarrow f$ peaks at higher frequency.

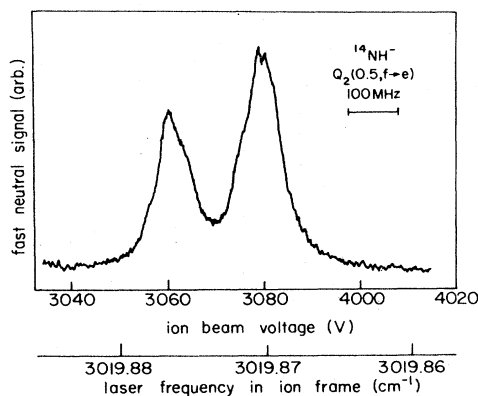


FIG. 6. Experimental line shape of the Q_2 (0.5) $f \rightarrow e$ transition.

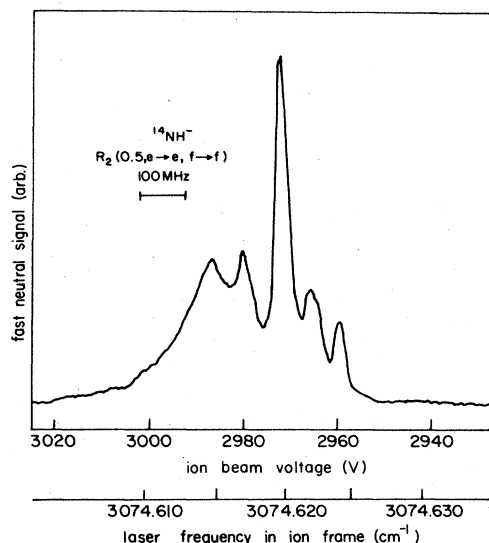


FIG. 7. Experimental line shape of the $R_2(0.5) e \rightarrow e$ and $f \rightarrow f$ transitions.

Line intensities

The intensity $I(J'')$ is

$$I(J'') = CS_J \exp[-B''J''(J''+1)/kT], \quad (25)$$

where C is a constant, T is the temperature, and S_J is the Hönl-London factor, given by²⁸

$$S_J^R = (J''+1+\Lambda'')(J''+1-\Lambda'')/(J''+1), \quad (26)$$

$$S_J^Q = (2J''+1)\Lambda''^2/J''(J''+1), \quad (27)$$

and

$$S_J^P = (J''+\Lambda'')(J''-\Lambda'')/J''. \quad (28)$$

These formulas are an approximation for a $^2\Pi$ state. They may be affected by the change of the angular momentum coupling case as J increases, but they are required for evaluation of the temperature.

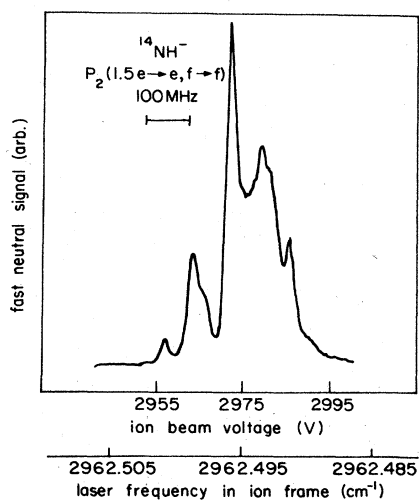


FIG. 8. Experimental line shape of the $P_2(1.5) e \rightarrow e$ and $f \rightarrow f$ transitions.

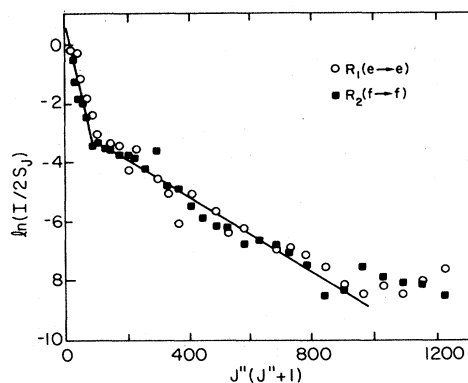


FIG. 9. Intensities of R -branch transitions, normalized to the ion-beam current and laser power. The slope of the curve gives a rotational temperature of ~ 500 K at low J'' and ~ 1800 K at high J'' .

Figure 9 displays $\ln(I/2S_J)$ as a function of $J''(J''+1)$ for the narrow R -branch lines. The intensity I has been normalized to the ion current and laser power. The uncertainty in individual data points is about 5–10% due to the change in the overlap between the ion and laser beams. The data points in the range $1.5 \leq J'' \leq 9.5$ yield a temperature of ~ 500 K. The data in the range $9.5 \leq J'' \leq 29.5$ yield ~ 1800 K. For higher J'' values, the data points level off, giving an even higher temperature. Figure 10 displays the same function for the narrow Q -branch lines. The temperature is consistent with the result from the R -branch data over the same range of J'' values. The low- J ions are rotationally “warm” (~ 500 K), with temperature characteristic of this type of ion source, while the high- J ions are rotationally “hot” (~ 1800 K).

The bimodal distribution is not surprising. It is well known that this kind of ion source is non-Boltzmannian. If ions come to equilibrium with the plasma in the source, they will have the temperature characteristic of the plasma. Based on the results in other ions, 500 K is a reasonable temperature for the plasma temperature. On the other hand, if the ions are extracted before coming to equilibrium, they will have nearly their nascent rotational distribution. We assume that the nascent distribution is rotationally hot, arising from the formation of NH^- from HN_3 . The low- J states of NH^- will equilibrate more rapidly than high- J states, for two reasons. (1) Each collision is more effective for low- J states. The rotational energy

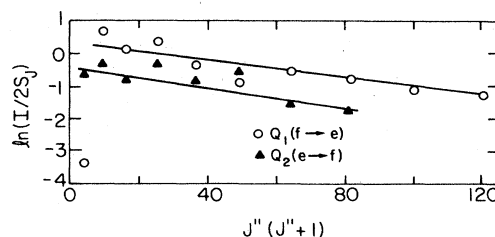


FIG. 10. Intensities of Q -branch transitions, normalized to ion-beam current and laser power. The slopes give rotational temperatures that agree with the temperature from the R -branch intensities, over the same range of J'' .

TABLE V. Observed intensity ratios for narrow resonance peaks in the R and Q branches and the ratios of the Hönl-London factors S_J .

Initial state		$\frac{R_1}{Q_1}$	$\frac{R_2}{Q_2}$	$\frac{S_f^R}{S_f^Q}$
J''	parity			
1.5	f		2.7	1.97
2.5	f	3.6	5.8	4.69
3.5	f	7.1	6.1	8.42
4.5	f	5.5	6.9	14.58
5.5	f	1.2	2.8	18.91
1.5	e	43.3	2.0	1.97
2.5	e	2.0	8.8	4.69
3.5	e	7.3	11.9	8.42
4.5	e	8.4	23.7	14.58
5.5	e	12.7	26.3	18.91
6.5	e	10.4		25.66
7.5	e	10.4		33.38

spacing BJ is small compared to kT for low J , but is of the order of 600 cm^{-1} for high J , and no longer small compared to kT . This makes J -changing collisions less effective for high J . (2) There are approximate selection rules limiting the change in J per collision, and high- J states must lose more angular momentum in order to come into equilibrium. Hence the population distribution has a rapidly equilibrating, low- J , low- T component and a slowly equilibrating high- J , high- T component.

The ratio of intensities in transitions sharing a common initial state is independent of the population of the initial state. The intensity ratios R_1/Q_1 and R_2/Q_2 are listed in Table V. Q_2 ($J''=0.5$) lines are omitted because each line consists of two groups of hyperfine components, which makes it hard to estimate the intensity. The value of R_1/Q_1 for transitions from $J''=1.5$ with parity e is much higher than all other values, while for the f parity the Q_1 line is missing. R_2/Q_2 is greater than R_1/Q_1 for most of the table. The intensity ratios generally increase with J , which is also true of the ratio of the Hönl-London factors. The peculiarity at $J=1.5$ can perhaps be explained from the transition between Hund's case (a) to case (b), which occurs at about that value of J . Alternatively, the Q_1 (1.5) transition may be anomalously low, because the upper state is barely above the autodetachment threshold.

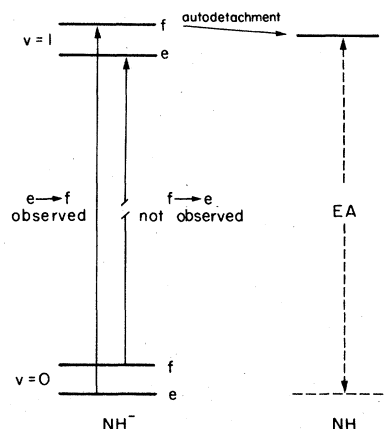


FIG. 11. Determination of the electron affinity of ^{14}NH . We observe the Q_1 (1.5, $e \rightarrow f$) transition but not the Q_1 (1.5, $f \rightarrow e$) transition. The most plausible explanation is that the e level does not autodetach because it lies below the lowest energy level of neutral NH. The resulting electron affinity of NH is $0.374\,362 \pm 0.000\,005 \text{ eV}$.

The electron affinity of NH

We observe P -branch and Q branch transitions to the $v=1$, $\Omega=\frac{3}{2}$, $J=1.5$ f level, but not to the e level of the same state (Fig. 11). This can be explained if the e level does not autodetach. The e level is the lowest-energy $v=1$ level of the ion. We assume that the lowest level of the neutral NH is energetically between the e and f levels of the ion. Of course, it is conceivable that there are other explanations for the nonappearance of both the Q_1 (1.5) $f \rightarrow e$ and the P_1 (0.5) $e \rightarrow e$ transitions, but our assumption is very plausible. Under this assumption, the Λ -doublet splitting places strict limits on the electron affinity. The E_{EA} of NH is between the observed Q_1 (1.5, $e \rightarrow f$) transition and the calculated Q_1 (1.5, $e \rightarrow e$) interval. This yields an E_{EA} of $3019.4077 \pm 0.0413 \text{ cm}^{-1}$, or $0.374\,363 \pm 0.000\,005 \text{ eV}$, using the conversion factor²³ $1 \text{ eV} = 8065.479 \text{ cm}^{-1} \pm 2.6 \text{ ppm}$.

The experimental and theoretical values for the E_{EA} are listed in Table VI. The electron affinity of NH was first measured experimentally from photoelectron spectrometry by Celotta, Bennett, and Hall⁴⁶ and Engelking and Lineberger,⁴⁷ who obtained 0.38 ± 0.03 and $0.381 \pm 0.014 \text{ eV}$, respectively. The best previous result

TABLE VI. Experimental and theoretical determinations of the electron affinity of NH (in eV).

E_{EA} (eV)	Expt./Theor.	Reference
0.38(3)	Expt.	Celotta <i>et al.</i> (Ref. 46)
0.381(14)	Expt.	Engelking and Lineberger (Ref. 47)
≤ 0.374	Expt.	Neumark <i>et al.</i> (Ref. 39)
0.374 362(5)	Expt.	This work
-0.25	Theor.	Rosmus and Meyer (Ref. 49) (PNO-CI) ^a
0.01	Theor.	Rosmus and Meyer (Ref. 49) (CEPA) ^b
0.22	Theor.	Cade (Ref. 48) (united atom)
0.37	Theor.	Cade (Ref. 48) (separated atom)

^aConfiguration interaction based on pseudonatural orbitals.

^bCoupled electron pair approximation.

was obtained by Neumark *et al.*,³⁹ who combined their experimental upper limit with the result of Engelking and Lineberger to obtain $E_{EA} = 0.370 \pm 0.004$ eV. Our work is better by a factor of 1000.

A reliable theoretical prediction of electron affinities is very difficult since the changes in the electron correlation energies caused by the attachment of an electron are of the same order of magnitude as the affinities themselves. Cade⁴⁸ obtained -1.55 eV as the value for the Hartree-Fock E_{EA} of NH. He suggested that the correlation-energy change caused by electron attachment may be approximated by the corresponding changes for the united atom or separated atom model. Applying the united-atom model to NH, he obtained an E_{EA} of 0.22 eV, whereas the separated-atom model yielded 0.37 eV. A different approach was followed by Rosmus and Meyer⁴⁹ to obtain uncorrected E_{EA} 's of -0.25 and $+0.01$ eV using two different wave functions. Unless the agreement is fortuitous, the separated-atom model yields the most reliable determination.

CONCLUSIONS

The work reported here, and in a previous publication,⁴⁵ greatly advances our knowledge of the spectrum of NH^- . We have more than doubled the number of high-resolution measurements, and have observed hyperfine structure and rotationally excited states in the autodetachment continuum. Line centers, linewidths, and intensities

have been measured in the *P*, *Q*, and *R* branches over a wide range of quantum numbers. A least-squares fit to the line centers has been performed and improved equilibrium spectroscopic constants extracted. This work makes NH^- one of the best explored negative molecular ions.

There are several possibilities for future work on this species. An isotopic substitution experiment on $^{15}\text{NH}^-$ can measure the anharmonicity of the potential well and the equilibrium vibrational frequency.⁶⁷ Analysis of the hyperfine structure would also be valuable.⁶⁸ The extensive data base should allow the determination of a realistic energy surface. We are pursuing these possibilities in our laboratory.

Note added in proof. CH_2CN^- has been studied by K. R. Lykke, D. M. Neumark, T. Andersen, V. J. Trapa, and W. C. Lineberger [in *Laser Spectroscopy VII*, edited by Y. R. Shen and T. W. Hänsch (Springer-Verlag, Berlin, 1985), pp. 130–133].

ACKNOWLEDGMENTS

We wish to express our thanks to Paul Engelking and John Hardwork for useful conversations. Financial support by the National Science Foundation and by the Chemical Physics Institute of the University of Oregon is gratefully acknowledged.

- ¹R. Wildt, *Astrophys. J.* **89**, 295 (1939); **93**, 47 (1941).
- ²B. Warner, *Mon. Not. R. Astron. Soc.* **137**, 119 (1967).
- ³P. A. Strittmatter and D. T. Wickramasinghe, *Mon. Not. R. Astron. Soc.* **152**, 47 (1971).
- ⁴J. E. Lovelock, R. J. Maggs, and E. R. Adlard, *Anal. Chem.* **43**, 1962 (1971).
- ⁵W. Gruebler, V. Koning, and P. A. Schmelzbach, *Nucl. Instrum. Methods* **86**, 127 (1970).
- ⁶T. de Jong, A. Dalgarno, and W. Boland, *Astron. Astrophys.* **91**, 68 (1980).
- ⁷E. Herbst and W. Klemperer, *Astrophys. J.* **185**, 505 (1973).
- ⁸W. D. Watson, *Rev. Mod. Phys.* **48**, 13 (1976).
- ⁹R. R. Corderman and W. C. Lineberger, *Annu. Rev. Phys. Chem.* **30**, 347 (1979).
- ¹⁰W. H. Wing, G. A. Ruff, W. E. Lamb, Jr., and J. J. Spezeski, *Phys. Rev. Lett.* **36**, 1488 (1976).
- ¹¹A. Carrington, *Proc. R. Soc. London, Ser. A* **367**, 433 (1979).
- ¹²T. Oka, *Phys. Rev. Lett.* **45**, 531 (1980).
- ¹³R. J. Saykally and R. C. Woods, *Annu. Rev. Phys. Chem.* **32**, 303 (1981).
- ¹⁴T. A. Miller, *Annu. Rev. Phys. Chem.* **33**, 257 (1982).
- ¹⁵J. Moseley and J. Durup, *Ann. Rev. Phys. Chem.* **32**, 53 (1981).
- ¹⁶K. M. Evenson, R. J. Saykally, D. A. Jennings, R. F. Curl, and J. M. Brown, in *Chemical and Physical Applications of Lasers V*, edited by C. B. Moore (Academic, New York, 1980), pp. 281ff.
- ¹⁷L. M. Branscomb, in *Atomic and Molecular Processes*, edited by D. R. Bates (Academic, New York, 1962), pp. 100–140.
- ¹⁸F. M. Page and G. C. Goode, *Negative Ions and the Magnetron* (Wiley, New York, 1969).
- ¹⁹R. S. Berry, *Chem. Rev.* **69**, 533 (1969).
- ²⁰B. Steiner, *Case Studies in Atomic Physics II*, edited by E. W. McDaniel and M. R. C. McDowell (North-Holland, Amsterdam, 1972), pp. 485–545.
- ²¹B. K. Janousek and J. I. Brauman, *Gas Phase Ion Chemistry*, edited by M. T. Bowers (Academic, Orlando, 1979).
- ²²H. S. W. Massey, *Negative Ions*, 3rd ed. (Cambridge University Press, London, 1976).
- ²³H. Hotop, and W. C. Lineberger, *J. Phys. Chem. Ref. Data* **14**, 731 (1985).
- ²⁴P. S. Drzaic, J. Marks, and J. I. Brauman, in *Gas Phase Ion Chemistry*, edited by M. T. Bowers (Academic, Orlando, 1984), Vol. 3, p. 167.
- ²⁵S. E. Novick, P. C. Engelking, P. L. Jones, J. H. Futtrell, and W. C. Lineberger, *J. Chem. Phys.* **70**, 2652 (1979).
- ²⁶G. Herzberg and A. Lagerqvist, *Can. J. Phys.* **46**, 2363 (1968).
- ²⁷W. C. Lineberger and T. A. Patterson, *Chem. Phys. Lett.* **13**, 40 (1972).
- ²⁸P. L. Jones, R. D. Mead, B. E. Kohler, S. D. Rosner, and W. C. Lineberger, *J. Chem. Phys.* **73**, 4419 (1980).
- ²⁹U. Hefter, R. D. Mead, P. A. Schulz, and W. C. Lineberger, *Phys. Rev. A* **28**, 1429 (1983).
- ³⁰P. A. Schulz, R. D. Mead, P. L. Jones, and W. C. Lineberger, *J. Chem. Phys.* **77**, 1153 (1982).
- ³¹K. R. Lykke, R. D. Mead, and W. C. Lineberger, *Phys. Rev. Lett.* **52**, 2221 (1984).
- ³²T. Andersen, K. R. Lykke, D. M. Neumark, and W. C. Lineberger, in *Proceedings of the XIV ICPEAC Conference*, edited by D. C. Lorents, W. E. Meyerhof, and J. R. Peterson (North-Holland, Amsterdam, 1986), pp. 791–798; *J. Chem. Phys.* (to be published). (See Note Added in Proof.)
- ³³Y. K. Bae, M. J. Coggiola, and J. R. Peterson, *Phys. Rev. Lett.* **52**, 747 (1984).
- ³⁴H. H. Michels, *Phys. Rev. Lett.* **52**, 1413 (1984).
- ³⁵J. C. Owrutsky, N. H. Rosenbaum, L. M. Tack, and R. J. Say-

- kally, *J. Chem. Phys.* **83**, 5338 (1985); N. H. Rosenbaum, J. C. Owrutsky, L. M. Tack, and R. J. Saykally, *ibid.* **84**, 5308 (1986).
- ³⁶L. M. Tack, N. H. Rosenbaum, J. C. Owrutsky, and R. J. Saykally, *J. Chem. Phys.* **84**, 7056 (1986).
- ³⁷D. J. Liu and T. Oka, *J. Chem. Phys.* **84**, 2426 (1986).
- ³⁸D. Rehfuss, M. W. Crofton, and T. Oka, *J. Chem. Phys.* **85**, 1785 (1986).
- ³⁹D. M. Neumark, K. R. Lykke, T. Andersen, and W. C. Lineberger, *J. Chem. Phys.* **83**, 4364 (1985).
- ⁴⁰W. H. Wing, G. A. Ruff, W. E. Lamb, and J. J. Spezeski, *Phys. Rev. Lett.* **36**, 1488 (1976).
- ⁴¹M. Dufay, M. Carré, M. L. Gaillard, G. Meunier, H. Winter, and A. Zaginski, *Phys. Rev. Lett.* **37**, 1678 (1976).
- ⁴²A. Carrington, and P. J. Sarre, *Mol. Phys.* **34**, 291 (1977).
- ⁴³B. A. Huber, P. C. Cosby, J. R. Peterson, and J. T. Moseley, *J. Chem. Phys.* **66**, 4520 (1977).
- ⁴⁴J. T. Moseley, R. E. Olson, and J. R. Peterson, *Case Stud. At. Phys.* **5**, 1 (1975).
- ⁴⁵M. Al-Za'al, H. C. Miller, and J. W. Farley, *Chem. Phys. Lett.* **131**, 56 (1986).
- ⁴⁶R. J. Celotta, R. A. Bennett, and J. L. Hall, *J. Chem. Phys.* **60**, 1740 (1974).
- ⁴⁷P. C. Engelking and W. C. Lineberger, *J. Chem. Phys.* **65**, 4323 (1976).
- ⁴⁸P. E. Cade, *Proc. Phys. Soc. London* **91**, 842 (1967).
- ⁴⁹P. Rosmus and W. Meyer, *J. Chem. Phys.* **69**, 2745 (1978).
- ⁵⁰U. Manz, A. Zilch, P. Rosmus, and H. J. Werner, *J. Chem. Phys.* **84**, 5037 (1986).
- ⁵¹M. Al-Za'al, H. C. Miller, and J. W. Farley, *Phys. Rev. A* **33**, 977 (1986).
- ⁵²M. Al-Za'al, doctoral thesis, University of Oregon, 1986.
- ⁵³Wheaton Inc., 1000 Tenth St., Millville, NJ 08332.
- ⁵⁴J. W. Farley, *Rev. Sci. Instrum.* **56**, 1834 (1985).
- ⁵⁵J. D. Jackson, *Classical Electrodynamics*, 2nd ed. (Wiley, New York, 1975), p. 522.
- ⁵⁶S. L. Kaufman, *Opt. Commun.* **17**, 309, (1976); S. M. Trujillo, R. H. Neynaber, and E. W. Rothe, *Rev. Sci. Instrum.* **37**, 1655 (1966).
- ⁵⁷R. D. Mead, doctoral thesis, University of Colorado, 1984.
- ⁵⁸G. Herzberg, *Molecular Spectra and Molecular Structure Vol. I: Spectra of Diatomic Molecules*, 2nd ed. (Van Nostrand Reinhold, New York, 1950).
- ⁵⁹J. M. Brown, J. T. Hougen, K. P. Huber, J. W. C. Johns, I. Kopp, H. Lefebvre-Brion, A. J. Merer, D. A. Ramsay, J. Ros-tas, and R. N. Zare, *J. Mol. Spectrosc.* **55**, 500 (1975).
- ⁶⁰J. P. Maillard, J. Chauville, and A. W. Mantz, *J. Mol. Spectrosc.* **63**, 120 (1976).
- ⁶¹J. M. Brown, M. Kaise, C. M. L. Kerr, and D. J. Milton, *Mol. Phys.* **36**, 553 (1978).
- ⁶²J. A. Coxon, K. V. L. N. Sastry, J. A. Austin, and D. A. Levy, *Can. J. Phys.* **57**, 619 (1979).
- ⁶³T. Amano, *J. Mol. Spectrosc.* **103**, 436 (1984).
- ⁶⁴R. N. Zare, A. L. Schmeltekopf, W. J. Harrop, and D. L. Al-britton, *J. Mol. Spectrosc.* **46**, 37 (1973); R. N. Zare, A. L. Schmeltekopf, D. L. Albritton, and W. J. Harrop, *J. Mol. Spectrosc.* **48**, 174 (1973).
- ⁶⁵P. R. Bevington, *Data Reduction and Error Analysis for the Physical Sciences* (McGraw-Hill, New York, 1969).
- ⁶⁶D. W. Marquardt, *J. Soc. Ind. Appl. Math.* **2**, 431 (1963).
- ⁶⁷H. C. Miller and J. W. Farley, *J. Chem. Phys.* (to be published).
- ⁶⁸H. C. Miller, M. Al-Za'al, and J. W. Farley (unpublished).